Stability of Taylor–Couette flow in a finite-length cavity with radial throughflow

Eric Serre,[1] Michael A. Sprague,[2] and Richard M. Lueptow[3,a)]
[1]*LMSNM, CNRS—Universités d'Aix-Marseille, IMT, La Jetée-Technopôle de Chtâteau-Gombert, 38 rue Frédéric Joliot-Curie, 13451 Marseille Cedex 20, France*
[2]*School of Natural Sciences, University of California, Merced, California 95344, USA*
[3]*Department of Mechanical Engineering, Northwestern University, Evanston, Illinois 60208, USA*

(Received 13 November 2007; accepted 1 February 2008; published online 18 March 2008)

Linear stability analysis predicts that a radial throughflow in a Taylor–Couette system will alter the stability of the flow, but the underlying physics for the stabilization of the flow is unclear. We investigate the impact of radial inflow and outflow on Taylor vortex flow and wavy vortex flow in a finite-length cavity via direct numerical simulation using a three-dimensional spectral method. The numerical simulations are consistent with linear stability predictions in that radial inflow and strong radial outflow have a stabilizing effect, while weak radial outflow destabilizes the system slightly. A small radial outflow velocity enhances the strength of the Taylor vortices resulting in destabilization of the base flow, whereas strong radial outflow and radial inflow reduce vortex strength, thus stabilizing the system. The transition to wavy vortex flow is unaffected by small radial outflow, but is stabilized for radial inflow. For strong radial outflow the wavy vortex flow includes localized dislocations in the vortex structure. © *2008 American Institute of Physics*.
[DOI: 10.1063/1.2884835]

I. INTRODUCTION

Couette flow between a rotating inner cylinder and a stationary outer cylinder becomes centrifugally unstable when the rotational speed exceeds a critical value resulting in toroidal Taylor vortices. However, if the inner and outer cylinders are porous and a radial throughflow is imposed, the stability is altered. Linear stability analysis for axisymmetric flow indicates that the flow is stabilized by a radial inward flow or strong radial outward flow, while a weak radial outward flow destabilizes the system slightly.[1–7] The physics underlying the stabilizing and destabilizing effects of radial throughflow is not established.

Apart from the fundamental interest in this issue is that one of the practical applications of Taylor–Couette flow, rotating filtration, is based on a radial flow at the inner cylinder of a Taylor–Couette cell.[8] Rotating filtration is used commercially for extracting plasma from whole blood,[9–11] and it has been proposed as a method for other filtration systems[12–23] as well as for reverse osmosis to purify water.[24–26] A rotating filter consists typically of a cylindrical porous inner cylinder rotating within a concentric nonporous stationary outer cylinder. A suspension enters the system at one end and travels axially in the annulus between the two cylinders. As it travels axially, pure fluid passes radially through the inner cylinder and can be removed via a hollow shaft. By the time the suspension reaches the opposite end of the annulus, it is highly concentrated. The key advantage of rotating filtration over other types of filtration is that the Taylor vortices constantly wash particles away from the inner cylinder, preventing them from plugging the pores of the membrane.[27,28] While radial throughflow between two porous cylinders is somewhat different from rotating filtration in which the outer cylinder is nonporous, it can provide insight into the fundamental physics that alter the stability of Taylor–Couette flow when a radial throughflow is present.

Little work has been done to understand how the instability arises in this flow or the nature of the vortical structure, other than linear stability analysis of the system with respect to two-dimensional perturbations. Linear stability analysis, however, only provides information about the conditions at which the transition from stable to unstable flow occurs. Furthermore, it is well known that three-dimensional instabilities arise in cylindrical Couette flow. It is likely that similar three-dimensional instabilities come about when a radial flow is imposed on the system, although the radial flow may alter the nature of the unstable flow.

In this paper, we use direct numerical simulation to examine the impact of radial throughflow on the stability of cylindrical Couette flow. We begin by considering the two-dimensional case: the transition from nonvortical to vortical flow in a finite-length Taylor–Couette cell. Using simulation results it is possible to examine the details of the flow field to probe the underlying physics that lead to a stabilizing or destabilizing effect on the flow. Next, we use three-dimensional direct numerical simulation to examine the situation where the Taylor number is above that for transition from nonvortical flow to nonwavy toroidal Taylor vortices, resulting in vortical structures that can be fully three-dimensional. This paper represents the first work done to investigate these three-dimensional vortical structures in cylindrical Couette flow when a radial flow is imposed.

a)Author to whom correspondence should be addressed. Electronic mail: r-lueptow@northwestern.edu. Telephone: 847-491-4265. Fax: 847-491-3915.

II. GEOMETRY AND NUMERICAL METHOD

An annular cavity between two finite-length concentric cylinders of inner and outer radii r_i and r_o is considered, with the inner cylinder rotating at angular speed Ω and the outer cylinder and endwalls stationary. All surfaces are no-slip, and the radial velocity is prescribed at the inner and outer cylinders as u_i and u_o, respectively. The velocity field (u,v,w) is described by the incompressible, three-dimensional Navier–Stokes equations written using cylindrical coordinates (r,θ,z) in an absolute frame of reference according to the velocity-pressure formulation. Characteristic parameters of the system are the Taylor number $\mathrm{Ta}=\Omega r_i d/\nu$ (sometimes called a rotating Reynolds number in this form), the radial Reynolds number $\alpha=u_i r_i/\nu$, the radius ratio $\eta=r_i/r_o$, and the aspect ratio $\Gamma=2h/d$, where ν is the kinematic viscosity, $2h$ is the distance between endwalls, and $d=r_o-r_i$. For all simulations, $\eta=0.85$, $\Gamma=20$, and necessarily $u_o=\eta u_i$.

For the numerical simulations, we employed a pseudospectral Chebyshev collocation method that is identical to that used in our previous work.[29–33] Time integration was accomplished with a second-order backward implicit Euler scheme for the linear terms and a second-order explicit Adams–Bashforth scheme for the nonlinear terms.[34] An improved projection algorithm was employed for velocity-pressure coupling.[35] The two-dimensional mesh grid was defined by the Gauss–Lobatto–Chebyshev collocation points with 21 and 121 being the number of points in the radial and axial directions, respectively. For simulations of higher-order transitions, a three-dimensional model was used with 96 equally spaced mesh points in the azimuthal direction; radial and axial grids were as in the two-dimensional model. The boundary conditions on the endwalls are complicated by the singularity at the junction between the endwalls and the inner cylinder where there is a jump in the azimuthal and radial velocities. To minimize the impact of these singularities on numerical solutions, the azimuthal and radial velocity profiles at the endwalls were set so that the velocities are no-slip except very near the singularity, where velocities exponentially change to those of the adjacent cylinder as discussed in Czarny *et al.*[30] Previous validation[29,30] has shown the method to be in good agreement with theory[36] and measurements.[37]

III. RESULTS

A. Axisymmetric results: Two-dimensional transitions

In the absence of radial throughflow, Couette flow in an infinite-aspect-ratio system will become unstable to axisymmetric counter-rotating vortices at $\mathrm{Ta}_c=108.31$,[36] where Ta_c is the critical Taylor number for $\alpha=0$. As discussed above, linear stability analysis indicates that radial throughflow ($\alpha\neq 0$) alters the stability of the system, stabilizing the flow for $\alpha<0$ and $\alpha>15.0$, and destabilizing the flow for $0<\alpha<15.0$. The minimum in the stability curve occurs at $\alpha=7.08$, for which $\mathrm{Ta}/\mathrm{Ta}_c=0.955$.

In comparing the simulation results to the stability curve, it is necessary to extract the exact value for α at which the transition from stable to unstable flow occurs, but this is complicated by the finite length of the system. As an example, consider simulations for radial inflow at $\mathrm{Ta}/\mathrm{Ta}_c=1.44$, for which the critical radial Reynolds number for transition is $\alpha=-15$ according to linear stability analysis.[5,6] Unlike an infinite-aspect-ratio system, weak vortical flow will be present for all $\mathrm{Ta}>0$ due to Ekman pumping at the endwalls,[30,37–41] which complicates the identification of stable or unstable flow. Figure 1 shows radial velocities associated with vortical motion due to Ekman pumping for $\alpha=-15.5$, where the maximum and minimum radial velocities decrease rapidly moving away from endwall located at $z/h=1$, and for $\alpha=-14.5$, where the maximum and minimum radial velocities are nearly constant regardless of distance from the endwall. The significant differences between the two finite-cylinder results allow us to label the flows for $\alpha=-15.5$ and $\alpha=-14.5$ as stable and unstable, respectively. Implementing this approach, we found the transition from stable to unstable flow for several values of α, as shown in Fig. 2. Excellent agreement with linear stability theory is evident, verifying the validity of our simulation results. Due to the finite length of the system, similar agreement is not expected for critical wavenumbers. For example, for $\alpha=-15$, the critical wavenumber of an infinite-aspect-ratio

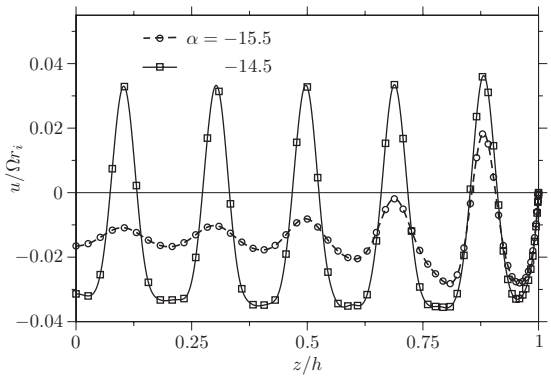

FIG. 1. Radial velocity in the upper-half of the cell at the midgap for $\alpha=-15.5$ and $\alpha=-14.5$ with $\mathrm{Ta}/\mathrm{Ta}_c=1.44$ and $\Gamma=20$. Symbols indicating nodal values are connected with Chebyshev polynomials.

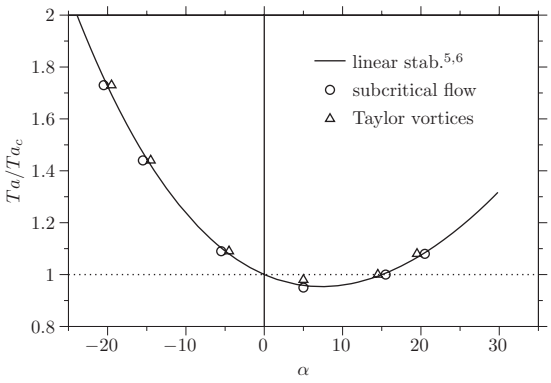

FIG. 2. Comparison of linear stability theory (Refs. 5 and 6) ($\Gamma\to\infty$) and axisymmetric computations ($\Gamma=20$) for the transition boundary between nonvortical and vortical flow.

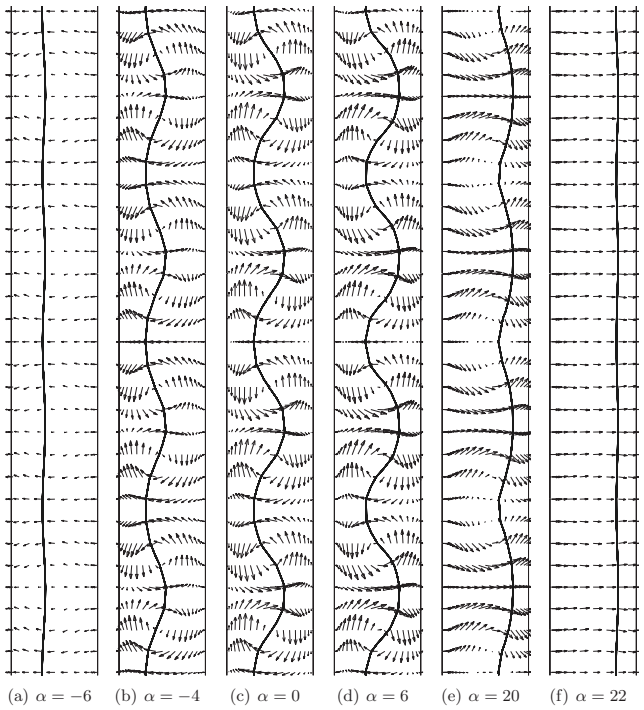

FIG. 3. Velocity vectors in the meridional plane for $|z/h| \leq 0.4$ for several values of the radial Reynolds number α with $\mathrm{Ta}/\mathrm{Ta}_c=1.1$ and $\Gamma=20$. In each subplot, the single contour corresponds to $v/\Omega r_i=0.50$; the inner cylinder is the left vertical line and the outer cylinder is the right vertical line.

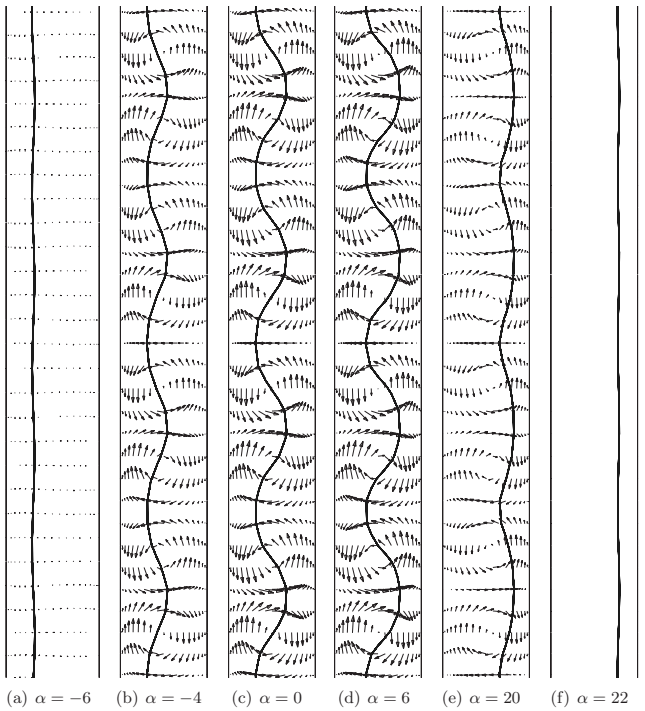

FIG. 4. Velocity vectors of Fig. 3 after subtracting the imposed mean radial velocity (at a given radius). In each subplot, the single contour corresponds to $v/\Omega r_i=0.50$; the inner cylinder is the left vertical line and the outer cylinder is the right vertical line.

system is $3.34d$,[6] whereas the wavenumber for $\alpha=-14.5$, $\mathrm{Ta}/\mathrm{Ta}_c=1.44$ in the finite system (Fig. 1) is $3.14d$, consistent with the finite aspect ratio that was imposed.

Although the stability curve in Fig. 2 serves as validation of the numerical method and provides information for the conditions under which transition occurs, it does not provide insight into the physics leading to the stabilizing effect of radial flow. To examine this, we consider velocity vector plots in a region around the cylinder midlength at $\mathrm{Ta}/\mathrm{Ta}_c=1.1$ and six values of α in Fig. 3. As the radial Reynolds number is increased from $\alpha=0$ to 6, the radial throughflow alters the vortices slightly, most readily visible in the slight outward tilt of the velocity vectors that were vertical at $\alpha=0$. Increasing the radial throughflow further to $\alpha=20$ increases the outward tilt of the velocity vectors, but more importantly, reduces the magnitude of the axial flow indicating weaker vortices. For $\alpha=22$, the vortices have disappeared altogether as the system reverts back to stable flow. The impact of radial inflow ($\alpha<0$) on the velocity field is similar. The velocity vectors at $\alpha=-4$ have a slight inward tilt compared to those at $\alpha=0$. However, when $\alpha=-6$, the vortices have nearly disappeared. The effect of the radial flow is also evident as a radial shift in the azimuthal flow, which is the dominant flow in the annulus. The single contour plotted in each frame of Fig. 3 corresponds to a dimensionless azimuthal velocity of $v/\Omega r_i=0.5$. For stable flow this contour would be a vertical straight line at $(r-r_i)/d=0.48$, approximately halfway across the gap. However, it is clear that not only is the contour distorted due to the vortical motion, it is shifted in the direction of the radial flow. In addition, the outward bulges in the contour have a greater axial extent than the inward bulges for radial outflow, suggesting that the imposed radial flow enhances the vortical outflow. Likewise, the inward bulges in the contour have a greater axial extent than the outward bulges for radial inflow, indicating enhancement of the vortical radial inflow.

When the radial flow is quite strong, such as the case when $\alpha=20$, the vortex structure is somewhat difficult to see, so it is useful to subtract the local imposed mean radial velocity (at a given radius) from the velocity field. As shown in Fig. 4, this makes the vortical structure more clear. Upon careful observation, it is evident that the vortex centers shift slightly in the direction of the radial throughflow, consistent with the shift in the relative amplitude of the perturbation velocities for the linear stability analysis.[5,6] The shift of the position of the $v/\Omega r_i=0.5$ contour is substantially larger than the shift in the position of the vortices themselves.

The radial shift of the vortices can be quantified based on the zero-crossing of the axial velocity profile in the radial direction at the middle of a vortex near the midlength of the annulus. The radial shift of the vortex position depends nearly linearly on the radial Reynolds number, as shown in Fig. 5. The outward radial shift of the vortices decreases slightly as the Taylor number increases, resulting in slightly different slopes for the relation for different Taylor numbers. The slope is steepest when the value for $\mathrm{Ta}/\mathrm{Ta}_c$ is close to the stability boundary, as is the case for $\mathrm{Ta}/\mathrm{Ta}_c=1$ for $\alpha>0$. This is most likely a result of the stronger influence of the imposed radial flow when the system is near the stability boundary than when it is not. Less data are available for

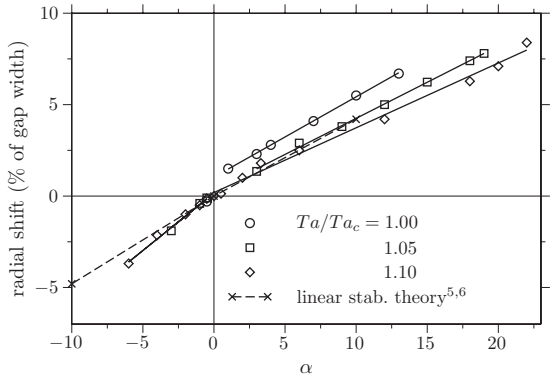

FIG. 5. The radial shift of vortices based on the zero-crossing of the axial velocity profile across the annulus at the center of a vortex near the midlength of the annulus as a function of the radial Reynolds number for $\Gamma=20$. Also shown is the shift predicted by linear stability theory (Refs. 5 and 6). The solid straight lines are linear least-squares fits to the data for each value of $\mathrm{Ta}/\mathrm{Ta}_c$ for $\alpha>0$ and for all values of $\mathrm{Ta}/\mathrm{Ta}_c$ for $\alpha<0$.

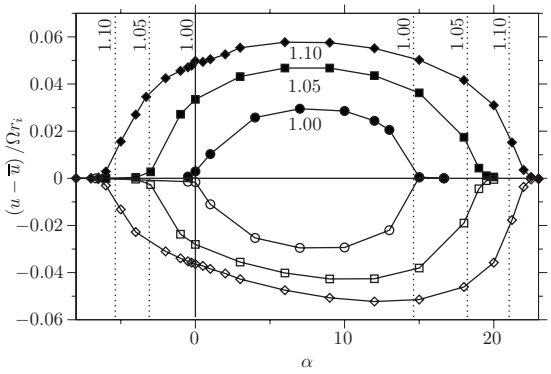

FIG. 6. The minimum (open symbols) and maximum (filled symbols) radial velocities relative to the mean radial velocity at the midgap in the region $|z/h|\leq 0.4$ as a function of the radial Reynolds number for $\mathrm{Ta}/\mathrm{Ta}_c=1.00$, 1.05, and 1.10 (numbers near curves) and $\Gamma=20$. The vertical broken lines indicate the stability boundaries according to linear stability theory (Refs. 5 and 6).

radial inflow ($\alpha<0$) at low values of $\mathrm{Ta}/\mathrm{Ta}_c$ because of the nature of the instability boundary, so it is difficult to ascertain if there are differences in the slope as $\mathrm{Ta}/\mathrm{Ta}_c$ is varied. The radial shift in the vortices is similar to that determined from the shift in the perturbation velocities according to the linear stability theory, as shown in Fig. 5. At transition to vortical flow for $\alpha=10$ (corresponding to $\mathrm{Ta}/\mathrm{Ta}_c=0.97$), the zero-crossing in the axial perturbation velocity is shifted by 4.2%, while for $\alpha=-10$ (corresponding to $\mathrm{Ta}/\mathrm{Ta}_c=1.25$), the zero-crossing is shifted by −4.8%.[6]

While the results presented to this point have clarified the nature of the vortical structure when a radial flow is imposed, our primary interest here is in how the radial flow alters the velocity field and affects the stability of the flow. A previous explanation[5,42] for the altered stability of the flow is based on the idea that the incipient instability first appears near the inner rotating cylinder[43,44] and propagates radially outward. The proposed explanation suggests that radial inflow or strong radial outflow could wash the fluid where the incipient instability occurs out of the annulus, thus stabilizing the flow, while a weak radial outflow promotes the instability by carrying the incipiently unstable fluid across the annulus. Of course, linear stability analysis does not predict a localized instability, but instead a global instability. The influence of the imposed radial flow on the velocity field, particularly the tilting of velocity vectors in the direction of the radial flow in Fig. 3 suggests that the competition between the imposed radial velocity and the radial velocity related to the Taylor vortices may better explain the stabilizing effect of the imposed radial flow.

Given that the radial velocity associated with the vortices is key to the stability of the flow, we plot the maximum and minimum dimensionless difference between the radial velocity and the imposed mean velocity $\bar{u}$ measured at the midgap $[r=(r_i+r_o)/2]$ in the central region $|z/h|\leq 0.4$ as a function of the radial Reynolds number in Fig. 6 for $\mathrm{Ta}/\mathrm{Ta}_c=1.0$, 1.05, and 1.1. Also included in this figure are vertical lines corresponding to the critical values of α for the onset of Taylor vortices according to linear stability theory.[5,6] The difference between the points where the relative maximum and minimum velocities are zero and the vertical broken lines for the linear stability boundaries is due to vortical motion induced by the Ekman vortices at the endwalls, which becomes more significant with increasing $\mathrm{Ta}/\mathrm{Ta}_c$.

Increasing the imposed radial outflow enhances the vortex strength (as measured by the maximum radial velocity) for $0<\alpha<7$. However, as the imposed outward radial flow increases further, the maximum radial velocity drops off, apparently due to the competition between the imposed outward radial flow and the radial flow of the vortex opposing it. Likewise, the imposed radial outflow first strengthens the vortices, evident as the minimum radial velocity grows in magnitude with increasing α for $0<\alpha<9-12$. For stronger radial outflow the magnitude of the minimum radial velocity decreases as the imposed radial flow stabilizes the system. The strength of the vortical flow decreases with increasing α until the flow becomes stable. The situation is somewhat different for an imposed inward flow ($\alpha<0$). In this case, the radial velocities due to the vortical flow continually decrease as the imposed inward radial flow increases (as α becomes more negative), indicating a stabilizing effect. This continues as α decreases until the vortices disappear.

The destabilizing effect of weak radial outflow for $0<\alpha<10$ and the stabilizing effect of radial inflow ($\alpha<0$) and strong radial outflow ($\alpha>10$) evident in Fig. 2 can be explained as follows. A small imposed radial outflow "encourages" the radial outflow portion of the vortices causing them to strengthen. For larger values of α, the imposed radial outflow competes with the radial inflow portion of the vortices. When α is increased further, the imposed radial outflow dominates and suppresses the vortex structure altogether. However, an analogous situation does not occur for radial inflow, where the imposed flow reduces the vortex strength even for small values of the imposed radial flow.

The effect of the radial flow on the stability could possibly be traced back to the nature of perturbations that result in the unstable flow. The Rayleigh inviscid approach to the stability is based on the idea that the flow becomes unstable

when the inward pressure gradient restoring force is not balanced by the outward inertia of the fluid. For inviscid flow, this results in the flow being unstable to axisymmetric disturbances at all radii for an inner cylinder rotating within a stationary outer cylinder. Of course, Taylor showed that viscosity stabilizes the flow at low Taylor numbers. Returning to the inviscid analysis, a fluid particle perturbed outward from its initial radius will move to a region where the local restoring force due to the pressure gradient at the infinitesimally larger radius is slightly less than the outward inertia of the particle, which is based on the particle's initial position. As a result, a fluid particle perturbed outward will continue outward. Likewise, a fluid particle perturbed inward from its initial radius will move to a region where the local restoring force due to the pressure gradient at the infinitesimally smaller radius is slightly greater than the outward inertia of the particle related to the particle's initial position, so a fluid particle perturbed inward will continue inward. The assumption, of course, is that it does not matter if the perturbation is inward or outward because continuity guarantees a return flow forming a vortex of Taylor–Couette flow.

Now consider the situation in more detail. One can show that, for the same perturbation magnitude, an inward perturbation results in slightly larger imbalance between the inertia and the restoring force than an outward perturbation. With no radial flow, this does not make any difference—either an inward or outward perturbation results in instability. Consider now an imposed radially inward flow. The imposed inward flow can "offset" a weak outward perturbation causing the flow to be more stable. A small imposed outward flow can "help" the weaker outward perturbation, causing the flow to become unstable more easily. On the other hand, a stronger outward flow, while helping the weak outward perturbation, also "offsets" the stronger inward perturbation making the flow more stable. This argument, of course, is mere handwaving at best. Nevertheless, it may provide some insight into the physics behind the nature of the stability curve.

Returning to the idea that radial flow in the vortex matches that of the imposed flow at the point the flow stabilizes as shown in Fig. 6, one should be able to estimate the value of radial velocity necessary to stabilize the flow. For conditions similar to those simulated here, experiments indicate that the maximum radial inflow velocity in a Taylor vortex is $mr_i\Omega$, where $m \approx -0.02$ for $\mathrm{Ta}/\mathrm{Ta}_c = 1.01$ and $m \approx -0.04$ for $\mathrm{Ta}/\mathrm{Ta}_c = 1.22$.[45] The imposed outflow radial velocity at the midgap of the annulus can be written as $2\alpha\nu\eta/r_i(1+\eta)$. Setting the sum of the vortical radial inflow velocity and the imposed radial outflow velocity equal to zero results in $\alpha = -m\,\mathrm{Ta}(1+\eta)/2(1-\eta)$. This expression provides an approximate value for α corresponding roughly to the situation where the radial velocity of the vortex is similar in magnitude to the imposed radial flow. Using $m=-0.02$ results in a predicted radial Reynolds number of outflow for transition of $\alpha \approx 13$, fairly close to the value predicted from linear stability of about 15 at $\mathrm{Ta}/\mathrm{Ta}_c = 1$. Using $m=-0.03$ for $\mathrm{Ta}/\mathrm{Ta}_c = 1.1$ results in a predicted radial Reynolds number for transition of $\alpha \approx 20$, fairly close to the value of about 22 from linear stability theory. This approach only works for imposed radial outflow, for which the flow is first destabilized as α increases from $\alpha=0$ and then stabilized as α increases further. For imposed radial inflow, the situation is different in that the flow is already more stable at $\alpha = 0$ than for small positive α. This is evident as the offset of the least stable situation to $\alpha \approx 7$ in Fig. 2. Because of this offset, the simple analysis outlined for imposed radial outflow does not accurately predict the critical value of α for radial inflow.

B. Three-dimensional results: Higher-order transitions

The Taylor number for transition from axisymmetric Taylor vortices to wavy vortices is not firmly established, even in the absence of radial flow. The transition to wavy vortex flow is predicted to occur at $\mathrm{Ta}/\mathrm{Ta}_c = 1.1$ for $\eta = 0.85$ for infinitely long cylinders.[46,47] For finite-length cylinders, experiments suggest a range of higher values for $\mathrm{Ta}/\mathrm{Ta}_c$ between 1.14 and 1.31 for $0.80 \leqslant \eta \leqslant 0.90$, depending on experimental conditions including the length of the apparatus,[45,48–52] and simulations for $\eta=0.87$ predict transition at $\mathrm{Ta}/\mathrm{Ta}_c = 1.8$ and 1.35 for $\Gamma=10$ and $\Gamma=20$, respectively.[51]

The simulation of the transition to higher-order unstable flows such as wavy-vortex flow is much more computationally difficult than the simulation of the transition from nonvortical to vortical flow, because the flow becomes three-dimensional and time dependent. As a result of the computational time involved in each simulation, it is challenging to map out the flow regimes that can occur in great detail. Nevertheless, we have developed a coarse map of the flow regimes that occur, with primary interest in the Taylor number at which the flow transitions from axisymmetric vortices to fully three-dimensional flow.

Three-dimensional simulations for $\alpha=0$ were initialized from two-dimensional simulation results for subcritical flow (with Ekman vortices due to the no-slip endwalls). The transition to wavy vortex flow occurred at $\mathrm{Ta}/\mathrm{Ta}_c \approx 1.32$ for $\alpha = 0$, consistent with numerical-simulation[51] and experimental[45,48–52] results. Simulations were performed for several values of $\mathrm{Ta}/\mathrm{Ta}_c$, where α was varied starting from $\alpha=0$ to locate transitions to different flow regimes. Four flow types were found using three-dimensional simulations, depending on the Taylor number and the radial Reynolds number: subcritical flow with Ekman vortices, axisymmetric Taylor vortex flow, wavy vortex flow (with four waves), and wavy vortex flow with dislocations. Figure 7 maps the conditions associated with the flow types for each of the simulations including the boundary for the first transition from subcritical stable flow to Taylor-vortex flow according to two-dimensional linear stability theory[5,6] (viz. Fig. 2). Also shown are approximate boundaries based on the numerical results for the second transition (to wavy-vortex flow) and the third transition (to wavy-vortex flow with dislocations). The general shape of the second stability boundary is similar to that for the first transition to vortical flow except that there is no destabilizing effect for small positive values of α. Thus, radial inflow stabilizes the transition to nonaxisymmetric

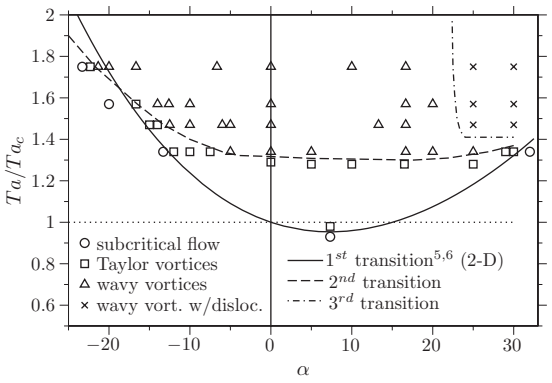

FIG. 7. Flow regime occurring under various parameters for three-dimensional simulations. Also shown is the two-dimensional linear stability boundary for the transition to Taylor-vortex flow (extrapolated for $\alpha > 30$), and the approximate stability boundaries for the transition to wavy-vortex flow and the transition to wavy-vortex flow with dislocations.

vortices, but radial outflow does not alter the stability until $\alpha \gtrsim 25$, when the flow is stabilized. The three-dimensional results indicate that the transition to wavy vortices occurs at a higher Taylor number than the transition to Taylor vortices for $-18 \lesssim \alpha \lesssim 30$. For $\mathrm{Ta}/\mathrm{Ta}_c = 1.75$ the transition from Taylor vortex flow to subcritical flow (with decreasing α) is shifted to a lower value of α than predicted by linear stability theory and our axisymmetric simulations (Fig. 2). This result was verified using extended-time simulations and higher resolution for the numerical model. The shift for the transition could be a result of hysteresis (decreasing α so the flow transitions from wavy to nonwavy to stable). The trends in the data for large positive α suggest that the three-dimensional flow may be less stable than two-dimensional flow for $\alpha > 30$, as well.

Examples of the three types of vortex structures occurring for $\mathrm{Ta}/\mathrm{Ta}_c = 1.47$ are shown in Fig. 8, visualized using the isosurface corresponding to $v/\Omega r_i = 0.50$. The vortices are axisymmetric for radial Reynolds numbers $-15 \lesssim \alpha \lesssim -13$, as shown in Fig. 8(a). Wavy vortices similar to those with no axial flow occur for $-13 \lesssim \alpha \lesssim 23$, as shown in Fig. 8(b). For $\alpha \gtrsim 23$, however, dislocations appear in the wavy

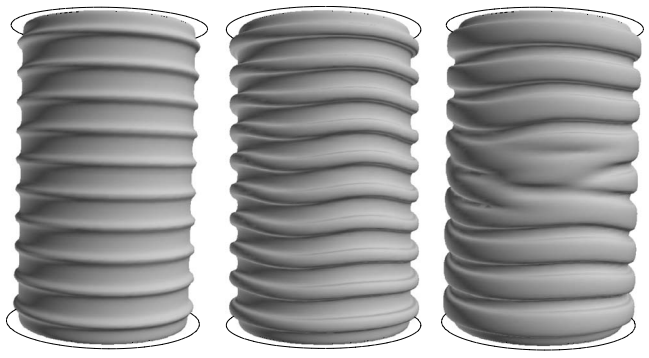

FIG. 8. Examples of vortex structures at $\mathrm{Ta}/\mathrm{Ta}_c = 1.47$ for (a) $\alpha = -15$ (axisymmetric Taylor vortices), (b) $\alpha = 13.3$ (wavy vortices), and (c) $\alpha = 30$ (wavy vortices with a single dislocation). Surfaces of $v/\Omega r_i = 0.50$ are shown.

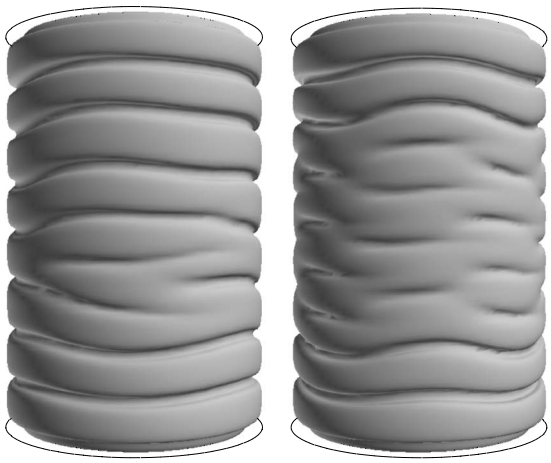

FIG. 9. Examples of wavy vortex structures with dislocations at $\alpha = 30$ for (a) $\mathrm{Ta}/\mathrm{Ta}_c = 1.57$ and (b) $\mathrm{Ta}/\mathrm{Ta}_c = 1.75$. Surfaces of $v/\Omega r_i = 0.50$ are shown.

vortices. In the case of $\alpha = 30$, there is a single dislocation that has a wave speed identical to that of the wavy vortices based on animations. Allowing the simulations to run for long times suggests that the dislocations come about following a transient secondary modulation of the waviness as the magnitude of the radial Reynolds number is increased. The dislocations are temporally stable, although they change somewhat in character over the duration of extended calculations as long as $2.14hd/\nu = 21d^2/\nu$. (This duration is somewhat longer than the times of $2hd/\nu$ and $10d^2/\nu$ that have been recommended as the times for onset and decay of Taylor vortices,[32] so we are reasonably sure that the dislocations do not result from the computations not achieving steady state.)

Other types of dislocations can occur as shown in Fig. 9 for $\alpha = 30$ and $\mathrm{Ta}/\mathrm{Ta}_c = 1.57$ and 1.75. As the Taylor number increases, the dislocations become more prevalent and appear at several locations in the annulus. For $\mathrm{Ta}/\mathrm{Ta}_c = 1.57$, there are two similar dislocations occurring on opposite sides of the cylinder; for $\mathrm{Ta}/\mathrm{Ta}_c = 1.75$, multiple dislocations are uniformly spaced around the cylinder and extend toward the endwalls.

Figure 10 shows velocity vector fields and contours of constant azimuthal velocity at several azimuthal slices through the dislocation corresponding to Fig. 8(c). The vortex centers are also shown based on the location of the local minimum velocity magnitude in the azimuthal plane. Starting with $\theta = 0$, there are six vortex centers marked, the lower two just below an outflow boundary where the dislocation eventually appears. With increasing θ, this outflow decreases in strength (as indicated by the azimuthal velocity contour being further from the outer wall for $\theta = 0.26$ than for $\theta = 0$) and becomes a weak inflow region (as indicated by the leftward bump in the azimuthal velocity contour) at $\theta = 0.52$. This inflow region is now associated with a new pair of weak vortices in what was originally the outflow region for $\theta = 0$. This is accompanied by a weakening of the adjacent vortex pairs above and below the new pair of vortices. These new

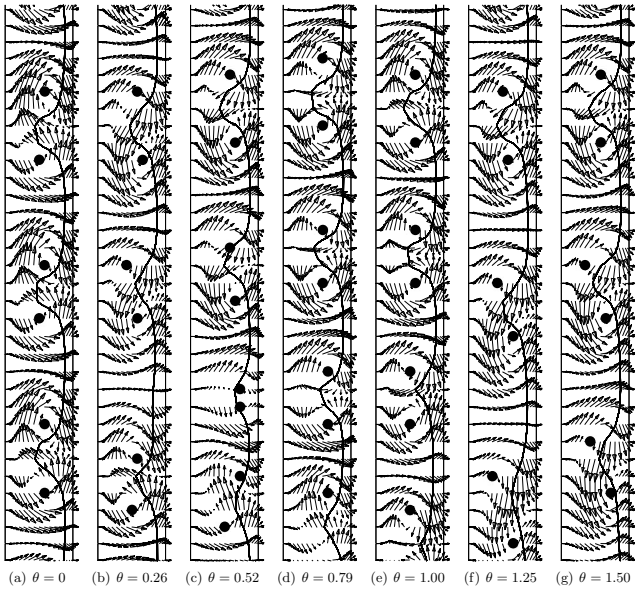

FIG. 10. Velocity vectors in several meridional planes for $|z/h| \leq 0.4$, slicing through the wavy-vortex dislocation for $\mathrm{Ta}/\mathrm{Ta}_c = 1.57$, $\alpha = 30$. In each subplot, the single contour corresponds to $v/\Omega r_i = 0.50$; the inner cylinder is the left vertical line and the outer cylinder is the right vertical line.

vortices are stronger at $\theta = 0.79$. The process reverses through the next azimuthal slices as the new pair of vortices disappears and the adjacent vortex pairs strengthen. By $\theta = 1.50$, the situation is very similar to that at $\theta = 0$. The weakening of the adjacent vortex pairs suggests that the imposed outflow disrupts these vortices allowing the new vortex pair to appear.

Returning to the general impact of the radial flow on the vortical structure, Fig. 11 shows velocity vectors in the meridional plane at $\theta = 0$ for $\mathrm{Ta}/\mathrm{Ta}_c = 1.47$ and several values of α. The radial shift of the flow is readily indicated by the shift of the azimuthal velocity contour corresponding to $v/\Omega r_i = 0.50$. As is the case for Taylor vortices, the stronger the radial flow, the greater the shift in this contour in the direction of the flow. Like the nonwavy vortices, the outward bulges in the contour grow in axial extent with increasing radial outflow as the imposed radial flow enhances the vortical outflow. Likewise, the inward bulges in the contour grow for radial inflow, indicating enhancement of the vortical inflow.

Of course, one of the inherent characteristics of wavy vortex flow is the speed at which the wavy vortex structure advances in the azimuthal direction. The wave speeds for wavy-vortex flow, c, based on Fourier analysis of the data at the midgap and noting that four waves occur around the circumference, are shown in Fig. 12 for four values of $\mathrm{Ta}/\mathrm{Ta}_c$. Also shown is the numerical/experimental result from Edwards *et al.*[51] for $\mathrm{Ta}/\mathrm{Ta}_c = 1.35$, $\Gamma = 20$, $\eta = 0.87$, which agrees well with our results. It is surprising that the wave speed is linearly dependent on the radial Reynolds number. Thus, radial inflow slows the azimuthal propagation of the waves, while radial outflow speeds it up. The wave speed of the dislocation is identical to the wave speed of the

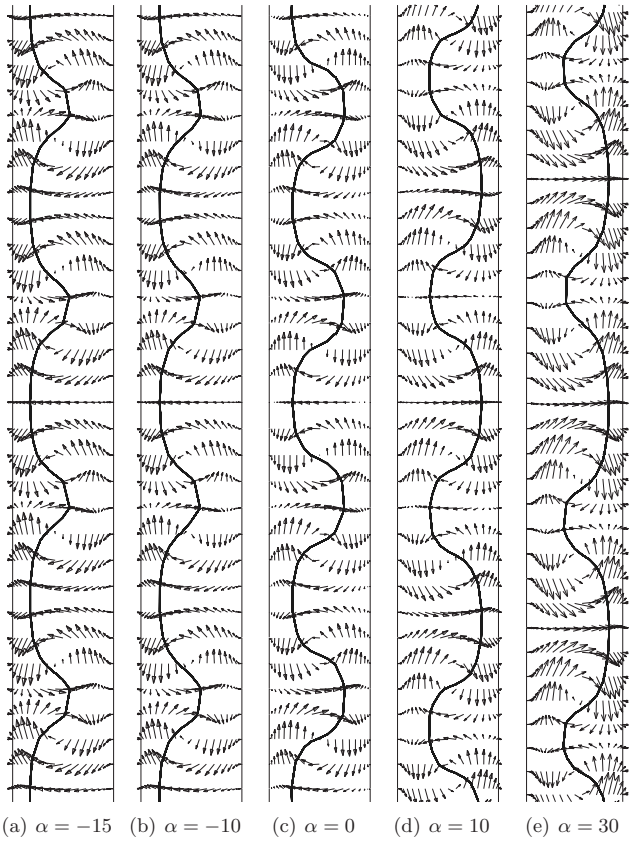

FIG. 11. Velocity vectors in the meridional plane at $\theta = 0$ for $|z/h| \leq 0.4$ for $\mathrm{Ta}/\mathrm{Ta}_c = 1.47$ demonstrating the vortical structure of the flow in the (a) absence and (b)–(d) presence of wavy vortices, and (e) with wavy vortices with a dislocation. In each subplot, the single contour corresponds to $v/\Omega r_i = 0.50$; the inner cylinder is the left vertical line and the outer cylinder is the right vertical line.

wavy structure. Furthermore, the wave speed is independent of $\mathrm{Ta}/\mathrm{Ta}_c$ for the range of Taylor numbers studied here.

Again the question arises about the underlying physics that cause the stabilization of the waviness with increasing magnitude of the radial Reynolds number, but the answer is not clear. We plot the maximum and minimum radial velocities as a function of the radial Reynolds number along with the imposed radial velocity in Fig. 13 for $\mathrm{Ta}/\mathrm{Ta}_c = 1.34$,

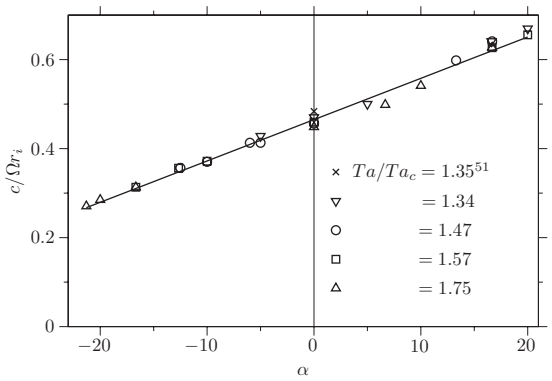

FIG. 12. Dependence of the wave speed for wavy-vortex flow on the radial Reynolds number for several $\mathrm{Ta}/\mathrm{Ta}_c$.

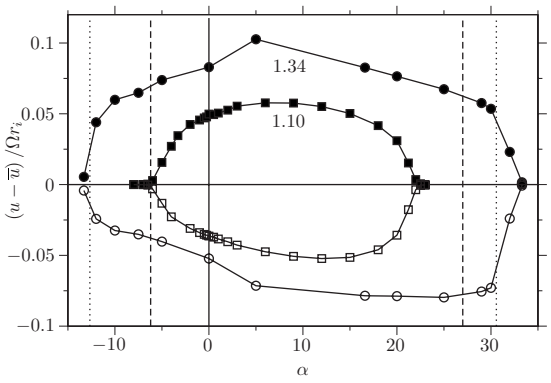

FIG. 13. The minimum (open symbols) and maximum (filled symbols) radial velocities relative to the mean radial velocity at the midgap in the region $|z/h| \leqslant 0.4$ as a function of the radial Reynolds number for $\mathrm{Ta}/\mathrm{Ta}_c = 1.10$ (viz. Fig. 6) and 1.34. The radial Reynolds numbers for transitions from stable to Taylor-vortex flow based on two-dimensional linear stability theory (Refs. 5 and 6) for $\mathrm{Ta}/\mathrm{Ta}_c = 1.34$ are indicated with vertical dotted lines. The vertical dashed lines indicate the boundaries of the approximate range of radial Reynolds numbers for wavy vortex flow at $\mathrm{Ta}/\mathrm{Ta}_c = 1.34$.

which is just above the transition to wavy vortex flow for $-5 \leqslant \alpha \leqslant 25$. The corresponding data for nonwavy vortices at $\mathrm{Ta}/\mathrm{Ta}_c = 1.10$ are shown for comparison. The dependence of the radial velocities on the radial Reynolds number is similar in character to that for the transition to Taylor-vortex flow, shown in Fig. 6, but it provides less insight. Again, a small imposed radial outflow enhances the strength of the vortices, while larger positive magnitudes of α and negative values of α correspond to reduced vortex strength. However, it is difficult to directly relate this to the appearance of wavy vortex flow, as was done for the transition to Taylor vortex flow.

IV. CONCLUSIONS

These simulations provide new insight into the connection between radial through-flow and the Taylor instability, as well as providing the first results for the transition to wavy vortices for the situation of an imposed radial flow. The vortex strength increases for small radial outflows leading to transition to vortical flow at a lower Taylor number than with no radial flow. But for larger radial outflow and any radial inflow the vortices are suppressed leading to a more stable situation than with no axial flow. For both radial inflow and radial outflow the vortices themselves and the azimuthal velocity isocontours are shifted in the direction of the flow a distance roughly proportional to the magnitude of the radial flow. This result was predicted from linear stability theory at the transition boundary between nonvortical and vortical flow, but has not been shown previously for Taylor numbers above the transition. Even when the flow becomes wavy, the vortices are similarly shifted in the direction of the radial flow.

Several question remain. The means by which the radial flow alters the stability of the transition from Taylor vortices to wavy vortices is still unclear. Further, the appearance of dislocations in the wavy vortex flow at high values of the radial Reynolds number is a curious phenomenon that may be related to the flow tending toward modulated wavy vortices. With regard to the practical motivation for this study, that of better understanding the flow physics in rotating filtration systems, this study is just a first step. In such a device, only the inner cylinder is porous, while the outer cylinder is nonporous. Thus, the next step is to model the system with an axial flow in the annulus to provide the source of the fluid that flows radially inward through the inner porous cylinder. However, this brings with it additional complexities from a simulation standpoint, including spatially varying axial and radial velocities in the annulus. Furthermore, it is well known that the imposition of an axial flow alters the stability of the Taylor–Couette flow.[6,43,44,53–62] In addition, when the vortices appear, they translate with the bulk axial flow,[36,57,63–67] leading to potential challenges in applying the appropriate boundary conditions at the entrance and exit for the axial flow, as well as the appropriate endwall boundary conditions. The three-dimensional simulations will also be challenging because of the appearance of helical vortices, wavy helical vortices, and higher-order vortical structures.[60,64,65,68–74] Apart from the computational challenges, while an axial flow has been shown to alter the stability of the Taylor–Couette flow based on both linear stability theory and experiments, the physics behind the flow stabilization has not been established, let alone how the interaction of an axial flow with the radial flow affects the stability.

ACKNOWLEDGMENTS

We gratefully acknowledge the financial support of Centre National de la Recherche Scientifique (CNRS). Much of this work was performed during visits by R.M.L. and M.A.S. to Laboratory MSNM at Université de la Méditerranée, funded by Direction Scientifique Sciences Pour l'Ingénieur of CNRS. The authors gratefully acknowledge Patrick Bontoux for making this collaboration possible. Thanks also to the scientific committee of the CNRS computing center (IDRIS) for supporting this work. M.A.S. acknowledges travel support provided by UC Merced faculty startup funds.

[1] T. S. Chang and W. K. Sartory, "Hydromagnetic stability of dissipative flow between rotating permeable cylinders," J. Fluid Mech. **27**, 65 (1967).
[2] T. S. Chang and W. K. Sartory, "Hydromagnetic stability of dissipative flow between rotating permeable cylinders. Part 2. Oscillatory critical modes and asymptotic results," J. Fluid Mech. **36**, 193 (1969).
[3] S. K. Bahl, "Stability of viscous flow between two concentric rotating porous cylinders," Def. Sci. J. **20**, 89 (1970).
[4] K. Bühler, in *Ordered and Turbulent Patterns in Taylor–Couette Flow*, edited by E. D. Andereck and F. Hayot (Plenum, New York, 1992), pp. 89–96.
[5] K. Min and R. M. Lueptow, "Hydrodynamic stability of viscous flow between rotating porous cylinders with radial flow," Phys. Fluids **6**, 144 (1994).
[6] E. C. Johnson and R. M. Lueptow, "Hydrodynamic stability of flow between rotating porous cylinders with radial and axial flow," Phys. Fluids **9**, 3687 (1997).
[7] A. Kolyshkin and R. Vaillancourt, "Convective instability boundary of Couette flow between rotating porous cylinders with axial and radial flow," Phys. Fluids **9**, 910 (1997).
[8] S. Lee and R. M. Lueptow, "Rotating membrane filtration and rotating reverse osmosis," J. Chem. Eng. Jpn. **37**, 471 (2004).
[9] R. M. Lueptow and A. Hajiloo, "Flow in a rotating membrane plasma separator," Trans. Am. Soc. Artif. Intern. Organs **41**, 182 (1995).

[10]K. Ohashi, K. Tashiro, F. Kushiya, T. Matsumoto, S. Yoshida, M. Endo, T. Horio, K. Ozawa, and K. Sakai, "Rotation-induced Taylor vortex enhances filtrate flux in plasma separation," Trans. Am. Soc. Artif. Intern. Organs **34**, 300 (1988).
[11]G. Beaudoin and M. Y. Jaffrin, "Plasma filtration in Couette flow membrane devices," Artif. Organs **13**, 43 (1989).
[12]K. H. Kroner, V. Nissinen, and H. Ziegler, "Improved dynamic filtration of microbial suspensions," Bio/Technology **5**, 921 (1987).
[13]K. H. Kroner and V. Nissinen, "Dynamic filtration of microbial suspensions using an axially rotating filter," J. Membr. Sci. **36**, 85 (1988).
[14]S. Wronski, E. Molga, and L. Rudniak, "Dynamic filtration in biotechnology," Bioprocess Eng. **4**, 99 (1989).
[15]U. B. Holeschovsky and C. L. Cooney, "Quantitative description of ultrafiltration in a rotating filtration device," AIChE J. **36**, 1219 (1991).
[16]G. Belfort, J. M. Pimbley, A. Greiner, and K. Y. Chung, "Diagnosis of membrane fouling using a rotating annular filter. 1. Cell culture media," J. Membr. Sci. **77**, 1 (1993).
[17]G. Belfort, P. Mikulasek, J. M. Pimbley, and K. Y. Chung, "Diagnosis of membrane fouling using a rotating annular filter. 2. Dilute particle suspensions of known particle size," J. Membr. Sci. **77**, 23 (1993).
[18]H. B. Winzeler and G. Belfort, "Enhanced performance for pressure-driven membrane processes: The argument for fluid instabilities," J. Membr. Sci. **80**, 35 (1993).
[19]A. Margaritis and C. R. Wilke, "The rotorfermentor. I. Description of the apparatus, power requirements, and mass transfer characteristics," Biotechnol. Bioeng. **20**, 709 (1978).
[20]B. Hallström and M. Lopez-Leiva, "Description of a rotating ultrafiltration module," Desalination **24**, 273 (1978).
[21]W. Tobler, "Dynamic filtration—the engineering concept of the Escher Wyss pressure filter," Filtr. Sep. **15**, 630 (1979).
[22]W. Tobler, "Dynamic filtration: Principle and application of shear filtration in an annular gap," Filtr. Sep. **19**, 329 (1982).
[23]T. Murase, E. Iritani, P. Chidphong, K. Kano, K. Atsumi, and M. Shirato, "High speed microfiltration using a rotating, cylindrical ceramic membrane," Int. Chem. Eng. **31**, 370 (1991).
[24]S. Lee and R. M. Lueptow, "Rotating reverse osmosis for water recovery in space: Influence of operational parameters on RO performance," Desalination **169**, 109 (2004).
[25]S. Lee and R. M. Lueptow, "Model predictions and experiments for rotating reverse osmosis for space mission water reuse: A comparison," Sep. Sci. Technol. **39**, 539 (2004).
[26]T. N. Shah, Y. Yoon, C. L. Pederson, and R. M. Lueptow, "Rotating reverse osmosis and spiral wound reverse osmosis filtration: A comparison," J. Membr. Sci. **285**, 353 (2006).
[27]J. R. Hildebrandt and J. B. Saxton, *Bioprocess Engineering Colloquium* (The American Society of Mechanical Engineers, New York, 1987).
[28]J. A. Schwille, D. Mitra, and R. M. Lueptow, "Design parameters for rotating filtration," J. Membr. Sci. **204**, 93 (2002).
[29]O. Czarny, E. Serre, P. Bontoux, and R. M. Lueptow, "Spiral and wavy vortex flows in short counter-rotating Taylor–Couette cells," Theor. Comput. Fluid Dyn. **16**, 5 (2002).
[30]O. Czarny, E. Serre, P. Bontoux, and R. M. Lueptow, "Interaction between Ekman pumping and the centrifugal instability in Taylor–Couette flow," Phys. Fluids **15**, 467 (2003).
[31]O. Czarny, E. Serre, P. Bontoux, and R. M. Lueptow, "Ekman vortices and the centrifugal instability in counter-rotating cylindrical Couette flow," Theor. Comput. Fluid Dyn. **18**, 151 (2004).
[32]O. Czarny and R. M. Lueptow, "Time scales for transition in Taylor–Couette flow," Phys. Fluids **19**, 054103 (2007).
[33]E. Serre, E. C. del Arco, and P. Bontoux, "Annular and spiral patterns in flows between rotating and stationary discs," J. Fluid Mech. **434**, 65 (2001).
[34]J. M. Vanel, R. Peyret, and P. Bontoux, "A pseudospectral solution of vorticity-streamfunction equations using the influence matrix technique," in *Numerical Methods for Fluid Dynamics II*, edited by K. W. Morton and M. J. Baines (Clarendon, Oxford, 1986), pp. 463–475.
[35]I. Raspo, S. Hughes, E. Serre, A. Randriamampianina, and P. Bontoux, "A spectral projection method for the simulation of complex three-dimensional rotating flows," Comput. Fluids **31**, 745 (2002).
[36]A. Recktenwald, M. Lücke, and H. W. Müller, "Taylor vortex formation in axial through-flow: Linear and weakly nonlinear analysis," Phys. Rev. E **48**, 4444 (1993).
[37]V. Sobolik, B. Izrar, R. Lusseyran, and S. Skali, "Interaction between the Ekman layer and the Couette–Taylor instability," Int. J. Heat Mass Transfer **43**, 4381 (2000).
[38]T. A. DeRoquefort and G. Grillaud, "Computation of Taylor vortex flow by a transient implicit method," Comput. Fluids **6**, 259 (1978).
[39]G. Pfister and I. Rehberg, "Space-dependent order parameter in circular Couette flow transitions," Phys. Lett. **83A**, 19 (1981).
[40]G. Ahlers and D. S. Cannell, "Vortex-front propagation in rotating Couette–Taylor flow," Phys. Rev. Lett. **50**, 1583 (1983).
[41]D.-C. Kuo and K. S. Ball, "Taylor–Couette flow with buoyancy: Onset of spiral flow," Phys. Fluids **9**, 2872 (1997).
[42]K. Min and R. M. Lueptow, "Circular Couette flow with pressure-driven axial flow and a porous inner cylinder," Exp. Fluids **17**, 190 (1994).
[43]M. A. Hasoon and B. W. Martin, "The stability of viscous axial flow in an annulus with a rotating inner cylinder," Proc. R. Soc. London, Ser. A **352**, 251 (1977).
[44]N. Gravas and B. W. Martin, "Instability of viscous axial flow in annuli having a rotating inner cylinder," J. Fluid Mech. **86**, 385 (1978).
[45]S. T. Wereley and R. M. Lueptow, "Spatio-temporal character of non-wavy and wavy Taylor–Couette flow," J. Fluid Mech. **364**, 59 (1998).
[46]R. C. DiPrima, P. M. Eagles, and B. S. Ng, "The effect of radius ratio on the stability of Couette flow and Taylor vortex flow," Phys. Fluids **27**, 2403 (1984).
[47]C. A. Jones, "The transition to wavy Taylor vortices," J. Fluid Mech. **157**, 135 (1985).
[48]S. T. Wereley and R. M. Lueptow, "Azimuthal velocity in supercritical circular Couette flow," Exp. Fluids **18**, 1 (1994).
[49]C. D. Andereck, S. S. Liu, and H. L. Swinney, "Flow regimes in a circular Couette system with independently rotating cylinders," J. Fluid Mech. **164**, 155 (1986).
[50]D. Coles, "Transition in circular Couette flow," J. Fluid Mech. **21**, 385 (1965).
[51]W. S. Edwards, S. R. Beane, and S. Varma, "Onset of wavy vortices in the finite-length Couette–Taylor problem," Phys. Fluids A **3**, 1510 (1991).
[52]J. A. Cole, "Taylor-vortex instability and annulus-length effects," J. Fluid Mech. **75**, 1 (1976).
[53]J. Kaye and E. Elgar, "Modes of adiabatic and diabatic fluid flow in an annulus with an inner rotating cylinder," Trans. ASME **80**, 753 (1958).
[54]S. Chandrasekhar, "The hydrodynamic stability of viscid flow between coaxial cylinders," Proc. Natl. Acad. Sci. U.S.A. **46**, 141 (1960).
[55]R. C. DiPrima, "The stability of a viscous fluid between rotating cylinders with an axial flow," J. Fluid Mech. **9**, 621 (1960).
[56]K. Chung and K. Astill, "Hydrodynamic instability of viscous flow between rotating coaxial cylinders with fully developed axial flow," J. Fluid Mech. **81**, 641 (1977).
[57]B. Ng and E. Turner, "On the linear stability of spiral flow between rotating cylinders," Proc. R. Soc. London, Ser. A **382**, 83 (1982).
[58]K. Babcock, G. Ahlers, and D. Cannell, "Noise-sustained structure in Taylor–Couette flow with through flow," Phys. Rev. Lett. **67**, 3388 (1991).
[59]S. Chandrasekhar, "The stability of spiral flow between rotating cylinders," Proc. R. Soc. London, Ser. A **265**, 188 (1962).
[60]K. Schwarz, B. Springett, and R. Donnelly, "Modes of instability in spiral flow between rotating cylinders," J. Fluid Mech. **20**, 281 (1964).
[61]R. Donnelly and D. Fultz, "Experiments on the stability of spiral flow between rotating cylinders," Proc. Natl. Acad. Sci. U.S.A. **46**, 1150 (1960).
[62]M. Sorour and J. Coney, "The characteristics of spiral vortex flow at high Taylor numbers," J. Mech. Eng. Sci. **21**, 65 (1979).
[63]R. C. DiPrima and A. Pridor, "The stability of viscous flow between rotating concentric cylinders with an axial flow," Proc. R. Soc. London, Ser. A **366**, 555 (1979).
[64]D. Takeuchi and D. Jankowski, "A numerical and experimental investigation of the stability of spiral Poiseuille flow," J. Fluid Mech. **102**, 101 (1981).
[65]R. M. Lueptow, A. Docter, and K. Min, "Stability of axial flow in an annulus with a rotating inner cylinder," Phys. Fluids A **4**, 2446 (1992).
[66]S. T. Wereley and R. M. Lueptow, "Velocity field for Taylor–Couette flow with an axial flow," Phys. Fluids **11**, 3637 (1999).
[67]P. Büchel, M. Lücke, D. Roth, and P. Schmitz, "Pattern selection in the absolutely unstable regime as a nonlinear eigenvalue problem: Taylor vortices in axial flow," Phys. Rev. E **53**, 4764 (1996).

[68]H. Snyder, "Experiments on the stability of spiral flow at low axial Reynolds numbers," Proc. R. Soc. London, Ser. A **265**, 198 (1962).
[69]K. Bühler, "Instabilitaten spiralformiger stromungen im zylinderspalt," Z. Angew. Math. Mech. **64**, T180 (1984).
[70]K. Bühler and N. Polifke, *Dynamical Behaviour of Taylor Vortices with Superimposed Axial Flow* (Plenum, New York, 1990).
[71]K. Becker and J. Kaye, "Measurements of diabatic flow in an annulus with an inner rotating cylinder," J. Heat Transfer **84**, 97 (1962).
[72]K. Beranek, I. Streda, and J. Sestak, "On the flow of viscous liquids through annular clearances with the rotating inner cylinder," Acta Tech. CSAV **24**, 665 (1979).
[73]K. Kataoka, H. Doi, and T. Komai, "Heat/mass transfer in Taylor vortex flow with constant axial flow rates," Int. J. Heat Mass Transfer **20**, 57 (1977).
[74]C. Hoffmann, M. Lücke, and A. Pinter, "Spiral vortices and Taylor vortices in the annulus between rotating cylinders and the effect of an axial flow," Phys. Rev. E **69**, 056309 (2004).